https://doi.org/10.5194/egusphere-2024-1700
Preprint. Discussion started: 13 June 2024
© Author(s) 2024. CC BY 4.0 License.

Long-term changes in the thermodynamic structure of the lowermost stratosphere inferred from ERA5 reanalysis data

Franziska Weyland[1], Peter Hoor[1], Daniel Kunkel[1], Thomas Birner[2,3], Felix Plöger[4,5], and Katharina Turhal[4,5]

[1]Institute for Atmospheric Physics, Johannes Gutenberg University Mainz, Germany
[2]Meteorological Institute, Ludwig-Maximilians-University Munich, Germany
[3]Institute for Physics of the Atmosphere, Deutsches Zentrum für Luft- und Raumfahrt, Oberpfaffenhofen, Germany
[4]Institute of Energy and Climate Research, Stratosphere (IEK-7), Forschungszentrum Jülich, Jülich, Germany
[5]Institute for Atmospheric and Environmental Research, University of Wuppertal, Wuppertal, Germany

Correspondence: Franziska Weyland (franziska.weyland@uni-mainz.de)

Abstract. The lowermost stratosphere (LMS) plays an important role for stratosphere-troposphere coupling and the Earth's radiation balance. This study investigates the effects of long-term changes of the tropopause and the lower stratospheric isentropic structure on the mass of the LMS. We use ERA5 reanalysis data from 1979–2019, focusing on changes after 1998, which marks the anticipated beginning of stratospheric ozone recovery. The trend analysis is performed with a dynamic linear regression model (DLM), capable of modeling non-linear trends.

According to our study, isentropes in the lower stratosphere (here 380–430 K) show upward trends in the tropics and downward trends in the extratropics, consistent with a strengthening of the Brewer-Dobson circulation. In the Northern Hemisphere (NH), we find that the extratropical tropopause is rising at a mean rate of $-1\,\mathrm{hPa/decade}$. For the Southern hemispheric (SH) extratropics, the lapse rate tropopause shows a downward tendency of up to +2 $\mathrm{hPa/decade}$ after 1998. The tropical tropopause and the cold point is rising with an average trend of roughly $-0.5\,\mathrm{hPa/decade}$, consistent with increasing potential temperatures. Additionally, we find that the tropical tropopause in the NH has expanded polewards by $0.5°$ latitude.

Consistent with the upward and poleward trend of the NH tropopause, the mass of the LMS is decreasing by 2–3 % between 1998–2019 if a fixed isentrope (380 K) is chosen as the upper LMS boundary. This mass decline disappears if dynamical upper LMS boundaries are used, that take the upward trends of the tropical tropopause into account.

1 Introduction

The lowermost stratosphere (LMS), also referred to as stratospheric part of the "middle world", is defined as the region of the stratosphere where isentropic surfaces intersect with the tropopause (Holton et al., 1995). The "middle world" can be distinguished from the "overworld", where isentropes are situated entirely in the stratosphere, and the "underworld" with isentropes exclusively located in the troposphere (Hoskins, 1991). Along these intersecting isentropes, quasi-isentropic exchange between the tropical troposphere and the extratropical stratosphere is possible. The upper boundary of the LMS has often been approximated by the 380 K isentrope which, in turn, can be regarded as an approximation of the tropical tropopause (e.g., Appenzeller

https://doi.org/10.5194/egusphere-2024-1700
Preprint. Discussion started: 13 June 2024
© Author(s) 2024. CC BY 4.0 License.

et al., 1996; Schoeberl, 2004; Olsen et al., 2013; Wang and Fu, 2021).

The LMS includes the extratropical transition layer (ExTL) (WMO, 2003), which has been defined on the basis of trace gas gradient changes in the LMS (e.g. Hoor et al., 2004), consistent with trajectory studies (Berthet et al., 2007). The ExTL is characterized by irreversible mixing across the tropopause and high variability of radiatively relevant trace gases like water vapor and ozone (Pan et al., 2004; Hoor et al., 2002; Fischer et al., 2000). The ExTL partly coincides with the tropopause inversion layer (TIL) as marked by a maximum of static stability (Birner et al., 2002; Birner, 2006). Further, the ExTL region is characterized by strong shear occurrence just around the extratropical tropopause (Kunkel et al., 2019; Kaluza et al., 2021).

The LMS is essential for the Earth's radiation budget (e.g., Forster and Shine, 1997, 2002; Zhang et al., 2004; Riese et al., 2012) since it constitutes a region of strong composition gradients of, e.g., ozone and water vapor. Changes of the LMS composition affect local temperature gradients (e.g., Randel et al., 2007) with impacts on climate and circulation (e.g., Hegglin and Shepherd, 2009; Charlesworth et al., 2023). Furthermore, the LMS contains a significant proportion of stratospheric mass (ca. $20\,\%$), and thereby a considerable part of total column ozone, due to the exponential density decrease with altitude. LMS and stratospheric mass show a seasonal cycle, closely following the seasonal cycle of tropopause height (Appenzeller et al., 1996). On short time scales, LMS mass variations are linked to stratospheric-tropospheric mass exchange (e.g., Stohl, 2003; Schoeberl, 2004; Hegglin et al., 2010; Škerlak et al., 2014). This affects the abundance of trace gases such as ozone, which show sharp gradients in the UTLS. Due to this transport barrier property, which gives rise to strong trace gas gradients, the tropopause location is of special importance.

The LMS is bounded below by the extratropical tropopause. The location of the (extratropical) tropopause can be defined thermally based on the temperature lapse rate (WMO, 1957) or the potential temperature gradient (Tinney et al., 2022), dynamically by choosing a characteristic value of potential vorticity (PV) (e.g., Hoerling et al., 1991) or by PV gradients (Kunz et al., 2011), and chemically via trace gas gradients (e.g., ozone) or trace gas correlations (e.g., Bethan et al., 1996; Fischer et al., 2000). The tropical tropopause level, which may serve as an upper boundary for the LMS can be defined thermally by the (potential) temperature lapse rate or the cold point, i.e., the local temperature minimum (Holton et al., 1995), or as an isentrope, e.g., the potential temperature level of $380\,\mathrm{K}$.

Since the tropopause is strongly coupled to the temperature profile in the lower and middle atmosphere, the tropopause height is sensitive to climate changes and variability. Specifically, the tropopause height has been shown to be a robust fingerprint of anthropogenic climate change. Increasing concentrations of well-mixed greenhouse gases (GHG) lead to a warming of the troposphere and cooling of the stratosphere, reinforced by the depletion of stratospheric ozone. Warming of the troposphere and cooling of the stratosphere result in a tropopause rise (e.g., Seidel et al., 2001; Santer et al., 2004; Seidel and Randel, 2006). In addition to radiative effects, stratospheric dynamics, as manifested by the Brewer-Dobson circulation (BDC), affect the location of the tropopause and the equator-to-pole contrast in tropopause height (Birner, 2010b).

A rise of the global tropopause of the order of $-1\,\mathrm{hPa/decade}$ has been reported in many studies of radiosonde (e.g., Seidel and Randel, 2006; Xian and Homeyer, 2019; Meng et al., 2021) and satellite observations (e.g., Schmidt et al., 2008; Meng

https://doi.org/10.5194/egusphere-2024-1700
Preprint. Discussion started: 13 June 2024
© Author(s) 2024. CC BY 4.0 License.

et al., 2021) as well as in reanalysis data (e.g., Wilcox et al., 2012a; Xian and Homeyer, 2019) and climate models (e.g., Santer, 2003a) and for different tropopause definitions. Natural variability has been found to play a minor role in tropopause trends (Sausen and Santer, 2003; Meng et al., 2021). Instead, model experiments by Santer (2003b) suggest that $80\,\%$ of the tropopause rise between 1979–1999 are attributable to anthropogenic influence, primarily increasing greenhouse gas emissions and the resulting warming of the troposphere. The tropospheric warming was found to lead to a persistent lifting of the tropopause, despite the warming of the stratosphere due to the recovery of stratospheric ozone (Pisoft et al., 2021; Meng et al., 2021).

Cold point temperature trends in the tropics show large uncertainties, according to Tegtmeier et al. (2020), but suggest negative trends of -0.3 to $-0.6\,\mathrm{K/decade}$ based on the JRA-25, JRA-55, MERRA and MERRA2 reanalyses. The negative temperature tendency goes along with a tendency towards lower cold point pressure of the order of $-1\,\mathrm{hPa/decade}$. In ERA-Interim, on the other hand, the cold point temperature shows no trend ($0\,\mathrm{K/decade}$). The tropical tropopause layer (TTL) has been found to exhibit negative temperature trends of -0.5 to $-1\,\mathrm{K/decade}$ during the time period 1979–2005 based on reanalysis data and radiosonde observations (Tegtmeier et al., 2020).

The largest trends in tropopause height are usually apparent in the subtropics around the tropopause break, which can be associated with a transition from lower extratropical values to significantly higher levels characteristic for the tropical tropopause. This effect can be understood as a broadening of the tropics and has been observed in radiosonde and satellite data (e.g., Seidel and Randel, 2007; Meng et al., 2021) as well as reanalysis data (e.g., Lu et al., 2009; Birner, 2010a; Wilcox et al., 2012a). Xian and Homeyer (2019) find a dipole structure with regions of increasing and decreasing tropopause altitude around the mean tropopause break in different zonally resolved reanalyses for the time period 1981–2015. In latitude coordinates relative to the tropopause break, the dipole structure mostly disappears and tropopause trends become largest around the mean tropopause break which agrees with zonal mean analyses. Robust tropical widening has also been documented based on other metrics that, however, do not necessarily correlate well with variations in the location of the tropopause break (e.g., Staten et al., 2018; Grise et al., 2019). Turhal et al. (2024) report a tropical widening above $370\,\mathrm{K}$ and below $340\,\mathrm{K}$ but a narrowing of the tropospheric width in the region in between for the isentropic PV-gradient tropopause from reanalysis data between 1980–2017.

In addition to the observed long-term changes of the tropopause location, climate model projections agree on an acceleration of the Brewer-Dobson circulation (BDC) as a consequence of the greenhouse-gas induced climate change (e.g., Butchart, 2014). Stratospheric temperature changes linked to stratospheric ozone additionally influence the BDC evolution. In response to the increased tropical upwelling (extratropical downwelling), resulting in adiabatic cooling (heating), the temperature structure of the stratosphere is expected to change.

Observations of the BDC behavior are only possible indirectly and the different approaches give a less clear picture about recent BDC trends than model simulations. Thompson and Solomon (2009) for example, report trends of lower stratospheric temperature and ozone between 1979–2006 from satellite observations that agree with an increased BDC. Fu et al. (2019) use satellite observations of stratospheric temperatures to estimate an acceleration of the mean BDC by $1.7\,\%/\mathrm{decade}$ between

https://doi.org/10.5194/egusphere-2024-1700
Preprint. Discussion started: 13 June 2024
© Author(s) 2024. CC BY 4.0 License.

1980–2018 but a recent deceleration between 2000–2018, especially in the Southern hemisphere (SH). The temperature reduction in the tropical tropopause region and at the cold point reported by Tegtmeier et al. (2020) are consistent with increased tropical upwelling.

All in all, the thermodynamic structure of the lowermost stratosphere can be expected to change in response to increasing greenhouse gas concentrations and the recovery of stratospheric ozone (e.g. IPCC, 2023, Charlesworth et al., 2023). This study investigates the effect of long-term changes of the tropopause and the lower stratospheric potential temperature structure and their impact on the mass of the lowermost stratosphere on the basis of ERA5 reanalysis data. We focus on the time period after 1998, which marks the anticipated beginning of stratospheric ozone recovery.

The data and regression model used for this study are described in Sect. 2. Thereafter, Sect. 3 presents and discusses the results, divided into subsections concerning the temporal evolution of the tropopause (Sect. 3.1) and the lower stratospheric potential temperature structure (Sect. 3.2) as well as the mass of the lowermost stratosphere (Sect. 3.3). Sect. 3.3 is further divided into a consideration of the LMS boundary surfaces, an LMS climatology and LMS mass trends between 1998–2019. The final conclusions are presented in Sect. 4.

2 Data and methods

2.1 Data

For this study, ERA5 monthly mean data for the time period 1979–2019 has been used. We calculated the monthly mean data and the associated standard deviations from the hourly available ERA5 data. ERA5 has 137 hybrid sigma-pressure model levels in the vertical. In addition to the model level data, ECMWF provides the model data interpolated onto 37 pressure levels between $1000\,\mathrm{hPa}$ and $1\,\mathrm{hPa}$. On pressure levels, the vertical grid spacing in the UTLS is $25\,\mathrm{hPa}$ to $50\,\mathrm{hPa}$, which corresponds to roughly 600–$1200\,\mathrm{m}$. Furthermore, model data interpolated on the $2\,\mathrm{PVU}$ surface is available from ECMWF directly (Hersbach et al., 2020). We use ERA5 data on pressure levels and $2\,\mathrm{PVU}$ on a regular horizontal grid with a constant grid spacing of $0.25°$ in longitude and latitude.

2.2 Tropopause

To determine the lapse rate tropopause according to WMO (1957) from ERA5 data, we apply an algorithm closely following that of Birner (2010a), based on the work of Reichler et al. (2003). The algorithm identifies the lowest pressure level at which the lapse rate corresponds to $2\,\mathrm{K/km}$ (stratification threshold) and remains below this value on average for all higher levels within $2\,\mathrm{km}$ (thickness criterion). The search range is limited to 500–$75\,\mathrm{hPa}$, to avoid unreasonable values, for example due to surface inversions. At high latitudes, especially over the Antarctic continent in austral winter, it can be difficult to obtain a meaningful lapse rate tropopause due to weak stratification (Zängl and Hoinka, 2001). We therefore limit the tropopause

https://doi.org/10.5194/egusphere-2024-1700
Preprint. Discussion started: 13 June 2024
© Author(s) 2024. CC BY 4.0 License.

pressure at latitudes >50° to a minimum pressure of 150 hPa. If the detected tropopause pressure falls below this limit, the thickness criterion is suspended and the highest pressure (<500 hPa) corresponding to a lapse rate of 2 K/km represents the tropopause. Missing values are filled by bilinear interpolation. The detected lapse rate tropopause agrees well with the ERA-Interim lapse rate tropopause in Gettelman et al. (2010) and Wilcox et al. (2012b).

In addition to the thermal tropopause, a dynamical tropopause has been analyzed. ECMWF provides ERA5 model level data interpolated onto the 2 PVU isosurface which serves as the dynamical tropopause for this study. The 89 hPa isobar is taken as tropopause cap for cases when 2 PVU is below 89 hPa to avoid unreasonably large altitudes for the tropopause towards the equator (Hersbach et al., 2020; ECMWF, 2016).

Between 20°N–20°S, the cold point serves as an alternative metric to estimate the tropical tropopause (Holton et al., 1995). To deduce the cold point tropopause, we determine pressure and potential temperature at the level corresponding to a lapse rate of 0 K/km.

2.3 LMS mass

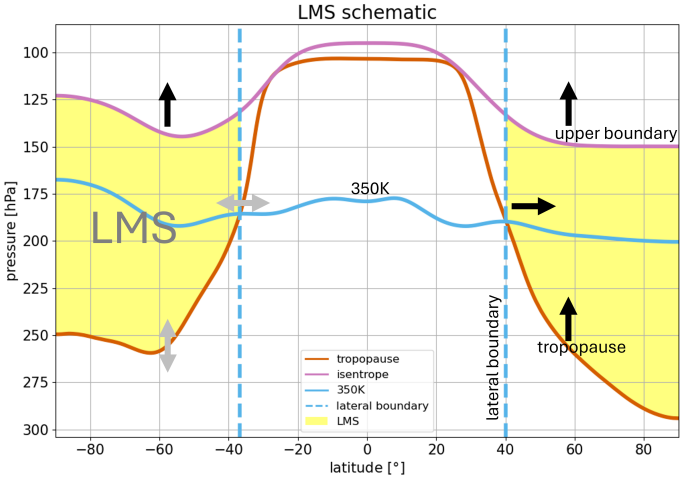

Figure 1. Schematic of the LMS. The LMS mass is enclosed by a lower boundary (tropopause, red) an upper boundary (purple) and a lateral boundary (blue vertical lines). The lateral boundary in this study is defined as the intersection between the tropopause and the 350 K isentrope, approximating the location of the subtropical jet streams and the maximum PV-gradient, marking a transport barrier. The arrows indicate the long term changes of the boundary surfaces, affecting the LMS mass as presented in Sect. 3.1 and 3.3.1. Figure 6 shows the location of the different LMS boundary surfaces compared in this study.

https://doi.org/10.5194/egusphere-2024-1700
Preprint. Discussion started: 13 June 2024
© Author(s) 2024. CC BY 4.0 License.

Following Appenzeller et al. (1996), the LMS mass $M(t)$ is obtained from the three dimensional integral of the pressure differences between the tropopause $p_1(\lambda, \Phi, t)$ and the pressure at the upper boundary $p_2(\lambda, \Phi, t)$ at every grid point and time step:

$$M(t) = \int_0^{2\pi} \int_{-\frac{\pi}{2}}^{\frac{\pi}{2}} \int_{p_1(\lambda,\Phi,t)}^{p_2(\lambda,\Phi,t)} -\frac{1}{g} dp \cos\Phi d\Phi d\lambda, \quad (1)$$

g is the gravity constant, λ is the longitude, Φ is the latitude and dp is the pressure difference. ERA5 data is used to calculate the LMS mass with respect to the lapse rate tropopause and the $2\,\mathrm{PVU}$ tropopause as the lower boundaries of the LMS.

Differing from most approaches, we will not only use a fixed isentropic value for the upper boundary of the LMS. Instead, in this study the upper LMS boundary surface depends on the potential temperature at the tropical tropopause. Therefore, we determine the pressure at the isentrope corresponding to the mean potential temperature at the tropical ($10°$N–$10°$S) lapse rate tropopause (PPT10mean) as well as at the cold point (PPTcp10mean) for every time step. In many LMS studies, the $380\,\mathrm{K}$ isentrope has been used to approximate of the upper LMS edge (e.g., Appenzeller et al., 1996; Wang and Fu, 2021). In this study, we compare $380\,\mathrm{K}$ with the dynamically defined upper boundaries (PPT10mean and PPTcp10mean).
The lateral LMS boundary in this study is defined as the latitude at which the respective monthly mean tropopause intersects with the $350\,\mathrm{K}$ isentrope. This intersection is determined by the sign change of the pressure difference between the tropopause and the isentrope. The latitude of intersection between the tropopause and $350\,\mathrm{K}$ roughly marks the location of the subtropical jet stream (e.g., Manney et al., 2011; Gettelman et al., 2011). Specifically, at $350\,\mathrm{K}$, the lapse rate tropopause and the $2\,\mathrm{PVU}$ surface are near the isentropic PV-gradient tropopause, a transport barrier separating the extratropical lower stratosphere from the tropical troposphere (Kunz et al., 2011; Turhal et al., 2024). The isentropic PV-gradient tropopause for the time period 1979–2019 was derived according to Turhal et al. (2024) and interpolated to pressure and potential temperature fields between $50°$N–$50°$S to be directly comparable to the lapse rate tropopause and $2\,\mathrm{PVU}$.

2.4 Regression tools

We use the dynamic linear regression model (DLM) by Laine et al. (2014) for the time series analyses in this study. The DLM has proved to be useful for trend estimation in many studies (e.g., Ball et al., 2017, 2018, 2019; Karagodin-Doyennel et al., 2022; Bognar et al., 2022) due to its ability to identify non-linear trends, smoothly varying in time without prior specification of possible inflection dates. The DLM decomposes the data time series into a non-linear background trend, a seasonal cycle composed of a 6 and a 12 months period and an autoregressive process. The user is able to add regressor variables, assessing causes of natural variability. For the DLM trend analyses in this study, we use regressors to account for El-Niño/Southern Oscillation (NOAA), the quasi-biennial oscillation at 30 and $50\,\mathrm{hPa}$ (FU-Berlin) as well as for stratospheric (volcanic) aerosol (Thomason et al., 2018). All regressors are normalized and, except SOAD, centered around zero.

The DLM is a Bayesian model based on the principles of Kalman filtering. The algorithm estimates the future system state

https://doi.org/10.5194/egusphere-2024-1700
Preprint. Discussion started: 13 June 2024
© Author(s) 2024. CC BY 4.0 License.

based on the previous estimates and the variance of the underlying data. The DLM uses an iterative process, based on the Markov chain Monte Carlo (MCMC) method, to infer possible system state time series from the Kalman algorithm outputs. Further details about the DLM can be found in Laine et al. (2014). The python based model code (dlmmc) is publicly available (Alsing, 2019).

In this study, the DLM runs provide 2000 possible model state estimates. The focus is on the hidden mean trend estimates. In the following, the DLM mean trend state time series is referred to as DLM trend state. The terms "trend" or "change" denote the DLM trend state difference between two dates, usually between January 1998 and December 2019. The fraction of DLM samples resulting in a negative (positive) change between two dates serves as evaluation of the confidence of the trend. The use of the term "statistical significance" refers to the probability of an overall decrease (increase) >95 % instead of frequentist significance tests. Ball et al. (2018, 2019) use this approach to evaluate their ozone trend analysis.

3 Structural changes in the lowermost stratosphere based on ERA5

3.1 Temporal evolution of the tropopause

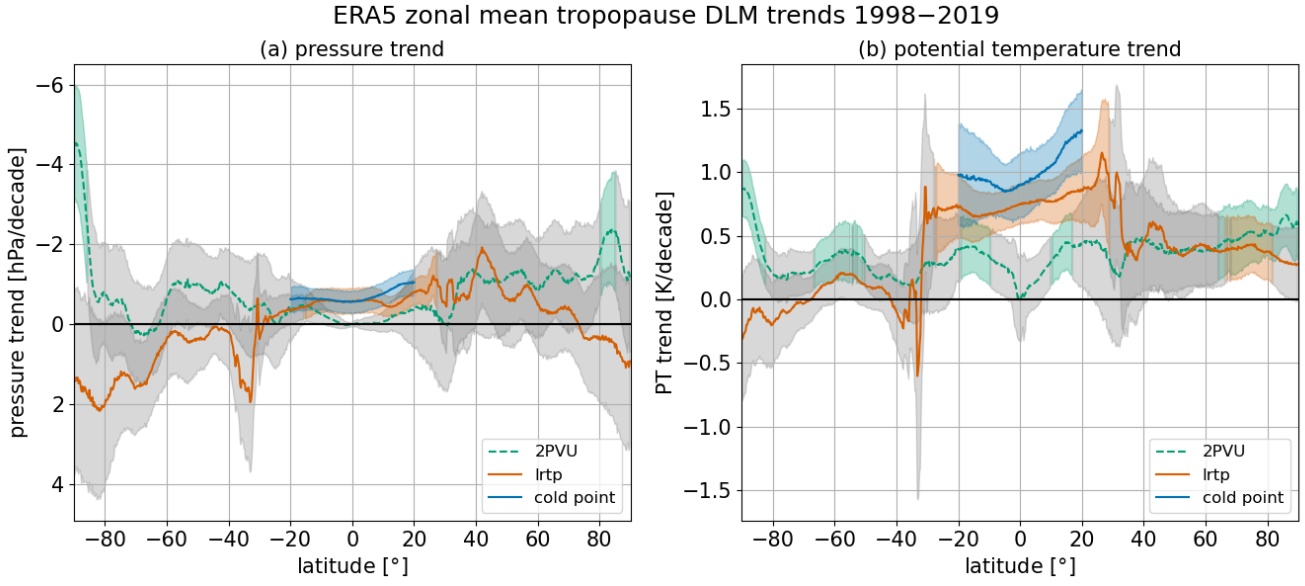

Figure 2. Zonal mean tropopause pressure (a) and potential temperature (b) trends between 1998–2019 as estimated by the DLM. Note that the pressure trend axis in (a) is inverted because decreasing pressure implies an upward trend. The lines show the mean DLM trends, the shading denotes the associated standard deviation. Colored shading highlights regions with trends of at least 95 % significance. Regions with grey shading are considered to show statistically insignificant trends. Red color is associated with the lapse rate tropopause, green color (dashed line) indicates the 2 PVU dynamic tropopause (capped at 89 hPa in the tropics) and blue color the cold point.

https://doi.org/10.5194/egusphere-2024-1700
Preprint. Discussion started: 13 June 2024
© Author(s) 2024. CC BY 4.0 License.

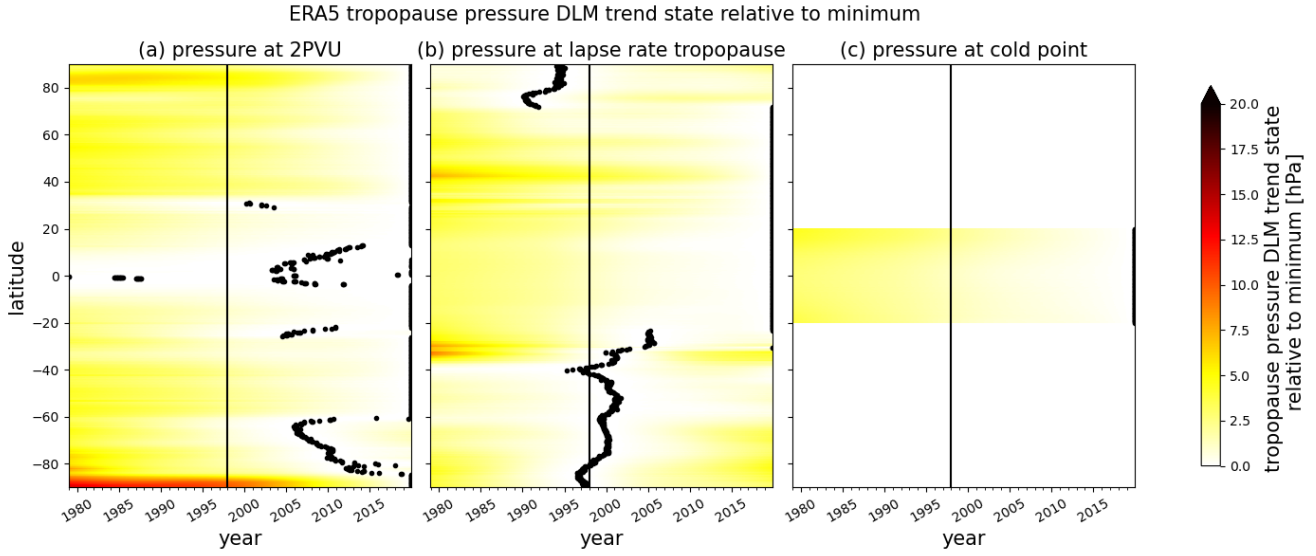

Figure 3. DLM trend state time series of pressure at the 2 PVU tropopasue (a), the lapse rate tropopause (b) and the cold point between 20°N–20°S (c) for the time period 1979–2019. The panels show the pressure trend state time series for all latitudes (y-axis). The minimum pressure trend state for every grid point is highlighted by the black dots and can indicate a trend reversal from decreasing to increasing pressure. The trend state time series are presented relative to the respective minimum but in absolute numbers [hPa] (color shading). The black vertical line marks the beginning of the year 1998.

Figure 2 shows the DLM trend results over the period 1998–2019 for the zonal mean tropopause pressure (a) and potential temperature (b). In the tropics and subtropics, the lapse rate tropopause pressure trends are negative and statistically significant (ca. $-0.5\,\mathrm{hPa/decade}$). Potential temperature trends in this region are more pronounced and statistically significant as well (ca. $0.7\,\mathrm{hPa/decade}$). Since the 2 PVU tropopause is capped at a fixed pressure of $89\,\mathrm{hPa}$ in the tropics, the respective pressure trends in the inner tropics are not meaningful.

In the NH mid-latitudes, both lapse rate tropopause and the 2 PVU dynamical tropopause show negative pressure trends of around $-1\,\mathrm{hPa/decade}$. This pressure decrease corresponds to a lifting of the tropopause and is consistent with the positive potential temperature trends. Similar tropopause trends have been reported by Wilcox et al. (2012a) for the time period 1989–2007 and Meng et al. (2021) for the time period 1980–2020.

In the SH mid-latitudes, on the other hand, the signs of the lapse rate tropopause and 2 PVU pressure trends differ at most latitudes. The SH mid-latitude lapse rate tropopause in this study generally shows positive pressure trends ranging between 0 and +2 $\mathrm{hPa/decade}$, corresponding to a sinking of the tropopause while 2 PVU pressure trends in this region amount to around $-0.8\,\mathrm{hPa/decade}$. A similar behavior of the SH mid-latitude lapse rate tropopause has been observed by Xian and Homeyer (2019) for the reanalyses JRA55, MERRA2 and CFSR. On the other hand, Xian and Homeyer (2019) do not observe such a downward trend of the SH mid-latitude lapse rate tropopause in ERA-Interim and it seems to oppose the findings by Wilcox

https://doi.org/10.5194/egusphere-2024-1700
Preprint. Discussion started: 13 June 2024
© Author(s) 2024. CC BY 4.0 License.

et al. (2012a) and Meng et al. (2021). However, it has to be noted that this study focuses on the tropopause changes after 1998. The non-linear DLM trend analysis for the entire time series 1979–2019 reveals a trend reversal of the lapse rate tropopause pressure around the year 2000 (Fig. 3b). Accordingly, the DLM results suggest an upward tendency of the SH mid-latitude lapse rate tropopause before the year 2000 and a downward tendency thereafter.

The positive pressure trends at the lapse rate tropopause above high latitudes could be the result of polar ozone recovery and associated increasing temperatures in the polar lower stratosphere (LS) after 1998. This is consistent with the minimum tropopause pressure DLM trend state in the polar regions, estimated around the time of ozone trend reversal (around the year 2000) (Fig. 3). A descent of the SH polar lapse rate tropopause has also been observed by Wilcox et al. (2012a) and in some of the reanalyses analyzed by Xian and Homeyer (2019). Moreover, the downward trend of the lapse rate tropopause at high and mid-latitudes could be linked to an acceleration of the BDC (Birner, 2010b). Indeed, age of air and long-lived trace gas measurements indicate an accelerating BDC in the SH after about the year 2000 (Strahan et al., 2020; Ploeger and Garny, 2022).

The zonal mean cold point shows a statistically significant pressure decrease of on average $-0.7\,\mathrm{hPa/decade}$, which is in agreement with findings of Tegtmeier et al. (2020). The upward tendency of the cold point is consistent with a potential temperature increase of on average $1\,\mathrm{K/decade}$.

3.2 Temporal evolution of the lower stratospheric potential temperature structure

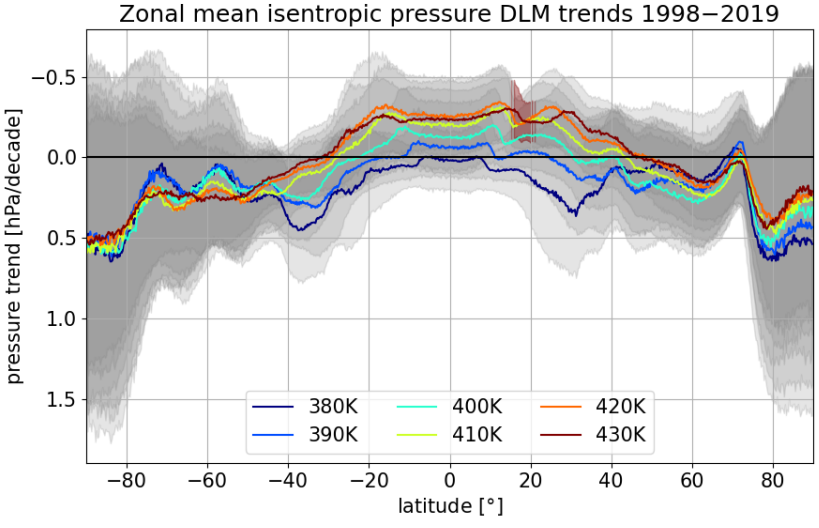

Figure 4. Zonal mean pressure trends at isentropes between 380–430 K as estimated by the DLM for the time period 1998–2019. The trends are given in hPa/decade. Note that the pressure trend axis is inverted because decreasing pressure implies an upward trend. Solid lines show the mean trend, the shading denotes the associated standard deviation. Colored shading marks regions with trends of at least 95 % significance. Regions with grey shading are considered to show statistically insignificant trends.

https://doi.org/10.5194/egusphere-2024-1700
Preprint. Discussion started: 13 June 2024
© Author(s) 2024. CC BY 4.0 License.

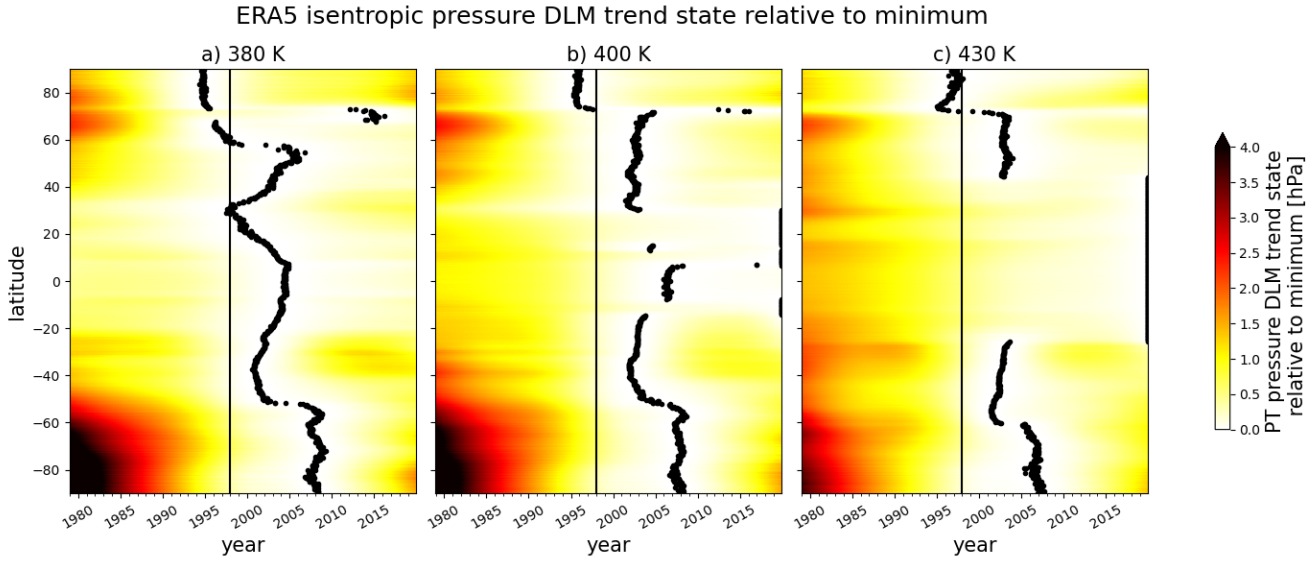

Figure 5. Isentropic pressure DLM trend state time series for the time period 1979–2019 at a) 380 K, b) 400 K and c) 430 K for all latitudes (y-axis). The minimum pressure trend state for every grid point is highlighted by the black dots and can indicate a trend reversal from decreasing to increasing pressure. The pressure trend state time series are presented relative to the respective minimum but in absolute numbers [hPa] (color shading). The black vertical line marks the beginning of the year 1998.

In addition to trends of the tropopause location, the location of isentropic surfaces is an important measure for structural changes of the UTLS region. Fig. 4 shows the pressure trend on isentropes between 380–430 K for the time period 1998–2019 as estimated by the DLM. The average pressure trends range between -0.3 to $+0.6\,\mathrm{hPa/decade}$, which corresponds to an absolute pressure change of up to 1 hPa during the 21 year period. The pressure trends between 380–430 K are positive in the extratropics, associated with decreasing altitude. In the tropics and subtropics, on the other hand, the pressure for the isentropes above 380 K is found to be decreasing, which corresponds to a rise of the respective potential temperature isosurfaces. However, the trends are hardly statistically significant. Rising of lower stratospheric isentropes in the tropics and sinking in the extratropics is consistent with a strengthened BDC which is associated with adiabatic cooling in the tropical LS and warming in the extratropical LS.

The magnitude of the isentropic pressure trend for a given latitude bin varies at different potential temperatures. Around 40°S for example, lower isentropes are sinking at a faster rate than higher ones. In the tropics and subtropics, higher isentropes are rising at a faster rate than lower ones. This indicates a weakening of the potential temperature gradient with pressure and accordingly a change of the stratification in the lower stratosphere. These lower stratospheric isentropic pressure trends could potentially be linked to TIL changes (e.g., Gettelman and Wang, 2015; Boljka and Birner, 2022), at least in the tropics. In the extratropics, tropopause and TIL are situated at lower potential temperature levels.

https://doi.org/10.5194/egusphere-2024-1700
Preprint. Discussion started: 13 June 2024
© Author(s) 2024. CC BY 4.0 License.

In addition to the average isentropic pressure trends between 1998–2019, it is worth considering the entire DLM trend state time series as the DLM is able to identify nonlinear trends (Fig. 5). In the extratropics, the DLM estimates an inflection point from decreasing to increasing pressure between the years 2000–2005 for all isentropes between 380–430 K. At SH high latitudes, isentropes reach their minimum pressure trend state later, between 2006–2008, but pressure changes are most pronounced in this region. Especially in SH high latitudes, the rise of isentropes between the 1980s an the 2000s is consistent with a cooling of the lower stratosphere due to ozone decline. Ozone recovery leads to a warming of the stratosphere, consistent with the descent of isentropes since the 2000s. This is in good agreement with the SH stratospheric temperature studies by Fu et al. (2019). In the SH high latitudes, this (potential) temperature increase is associated with a weakening of the SH polar vortex (Zambri et al., 2021), influencing polar winter ozone destruction and mixing of polar and mid-latitude air masses.

In the tropics and subtropics, a continuous rise of the isentropes above 390 K is evident. This is consistent with increased upwelling in the context of an enhanced BDC, associated with adiabatic cooling. Furthermore, diabatic cooling of the tropical lower stratosphere results from increasing GHG load in the troposphere and a continuous decline of lower stratospheric ozone. Such a cooling of the tropical stratosphere has been identified in observations (e.g., Scherllin-Pirscher et al., 2021) and reanalysis data (e.g., Tegtmeier et al., 2020).

https://doi.org/10.5194/egusphere-2024-1700
Preprint. Discussion started: 13 June 2024
© Author(s) 2024. CC BY 4.0 License.

3.3 The mass of the lowermost stratosphere

3.3.1 LMS boundary surfaces

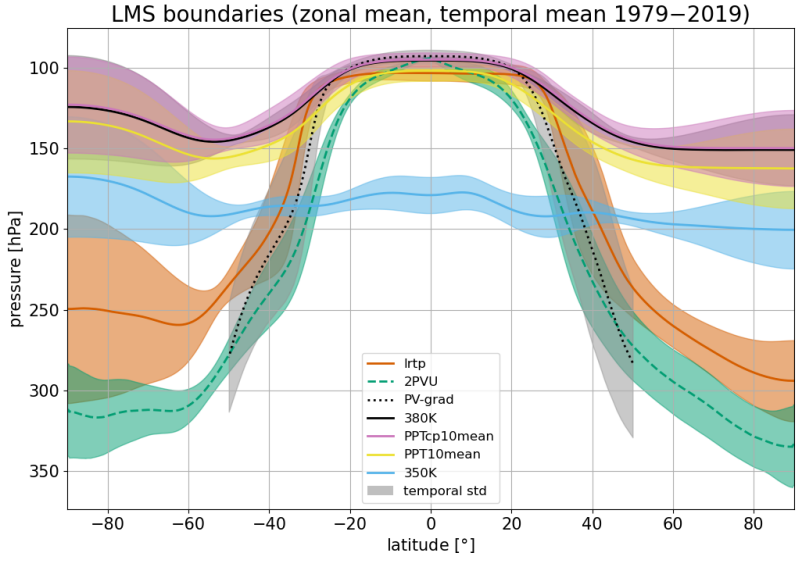

Figure 6. Zonal mean, temporal mean LMS boundaries between 1979–2019. The lines denote the mean location of the respective surfaces, the shading indicates the temporal standard deviation. The lower LMS boundary is defined by the lapse rate tropopause (red) or the 2 PVU dynamic tropopause (green, dashed line). The 380 K isentrope (black) can serve as the upper boundary. It is also possible to define dynamic upper boundaries depending on the potential temperature at the tropical tropopause. Here, the isentropes corresponding to the mean potential temperature between 10°N–10°S at the lapse rate tropopause (PPT10mean, yellow) and the cold point (PPTcp10mean, purple) are shown. The lateral LMS boundary can be approximated by the intersection between the 350 K isentrope (light blue) and the respective tropopause. This intersection is close to the isentropic PV-gradient tropopause (black, dotted line) at 350 K, which represents a transport barrier and serves as an approximation for the position of the subtropical jet stream.

The tropopause marks the lower boundary of the lowermost stratosphere (LMS). For the upper boundary, many studies choose the 380 K isentrope (e.g., Appenzeller et al., 1996; Wang and Fu, 2021). Wang et al. (2022) point out the importance to consider long term changes of the tropical tropopause location in different climates for LMS mass budget analyses. Their approach is to fit an isentrope between 360–390 K to the tropical lase rate tropopause. Similar to Wang et al. (2022), we define an upper LMS boundary with respect to the tropical lapse rate tropopause that allows for continuous variations of the boundary surface. To do so, we determine the mean isentropic pressure corresponding to the potential temperature at the tropical (10°N–10°S) lapse rate tropopause (PPT10mean). For comparison, we determine a second upper boundary surface based on the potential

https://doi.org/10.5194/egusphere-2024-1700
Preprint. Discussion started: 13 June 2024
© Author(s) 2024. CC BY 4.0 License.

temperature at the cold point (PPTcp10mean) in the same way. The different boundary surfaces used for LMS definition are displayed in Fig. 6.

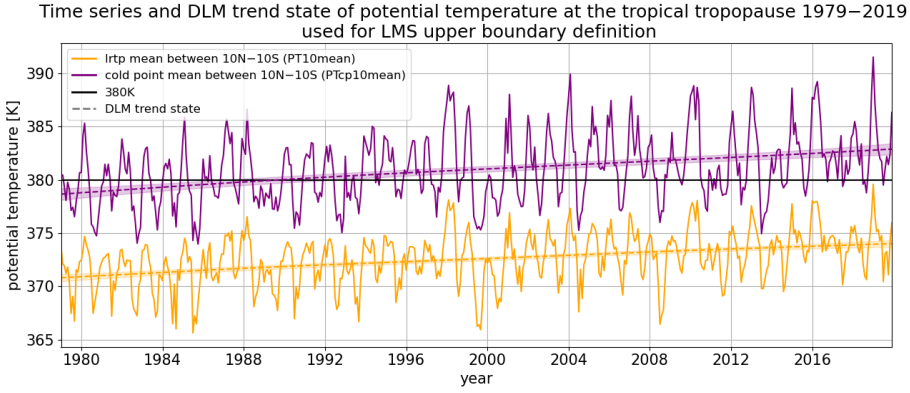

Figure 7. Temporal evolution of the potential temperature at the tropical tropopause between 1979–2019 as used for LMS upper boundary surface definition. Shown are the mean potential temperature between $10°$N–$10°$S at the lapse rate tropopause (PT10mean, yellow) and the cold point (PTcp10mean, purple). The black horizontal line marks 380 K. In addition to the time series (solid lines), the DLM trend state time series are depicted (dashed lines) together with the associated standard deviation (shading).

Fig. 7 and 8 show that a fixed upper LMS boundary (e.g., 380 K) cannot capture the variability and long-term evolution associated with the tropical tropopause. Specifically, the dynamically defined upper boundary surfaces (PPT10mean and PPTcp10mean)[1] show an opposite trend to the 380 K isentrope. This is due to the fact that the potential temperature at the tropical tropopause exhibits a positive trend (Fig. 7). For the mean potential temperature at the lapse rate tropopause between $10°$N–$10°$S, the DLM estimates an increase of 1.56 ± 0.33 K between 1998–2019. The temporal evolution of the potential temperature corresponding to the cold point amounts to 2.04 ± 0.61 K for the same time period. The potential temperature increase at the tropical tropopause leads to a global lifting of the defined upper LMS boundary surfaces (Fig. 8). The upward trends of the PPT10mean and PPTcp10mean surfaces are statistically significant for most latitudes in the tropics and mid-latitudes. The average trends of around $-1\,\mathrm{hPa/decade}$ are very similar to the trend of the 2 PVU tropopause and the lapse rate tropopause in in the NH mid-latitudes (Fig. 2). In the SH extratropics, the sign of the lapse rate tropopause pressure trend is opposite to that of the PPT surfaces.

Like the upper and lower LMS boundaries, the boundaries separating the LMS laterally from the TTL-region are allowed to vary dynamically with time. For this purpose, the intersections between the monthly mean tropopause and the 350 K isentrope are identified via the sign change of the pressure difference between both surfaces. This intersection serves as a proxy for the position of the subtropical jet stream (e.g., Manney et al., 2011; Gettelman et al., 2011). Specifically, the lapse rate tropopause and the 2 PVU surface at 350 K are close to the isentropic PV-gradient tropopause, which marks a clear transport barrier between the tropical troposphere and the extratropical lower stratosphere, i.e. the LMS (Kunz et al., 2011; Turhal et al., 2024).

[1]PPT10mean and PPTcp10mean: Pressure interpolated onto the isentrope corresponding to the potential temperature at the tropical lapse rate tropopause and the cold point, respectively.

https://doi.org/10.5194/egusphere-2024-1700
Preprint. Discussion started: 13 June 2024
© Author(s) 2024. CC BY 4.0 License.

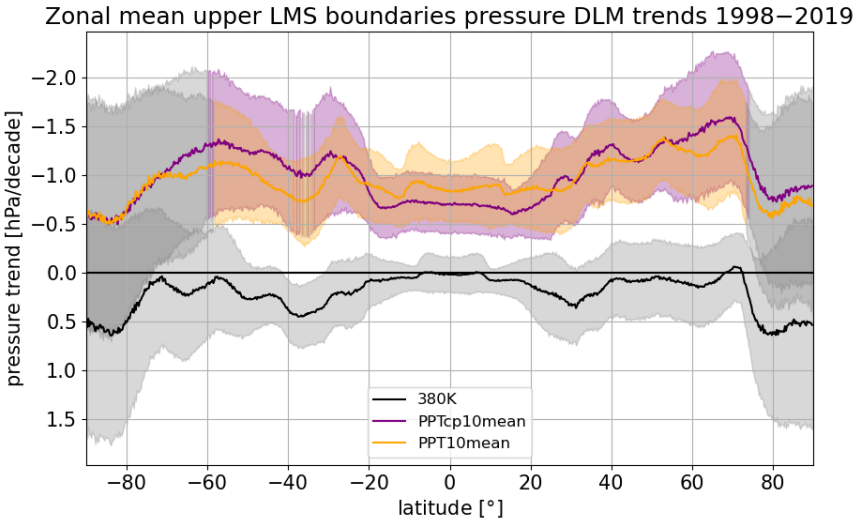

Figure 8. Zonal mean pressure trend at the LMS upper boundaries as estimated by the DLM for the time period 1998–2019. Shown are the isentropes corresponding to the mean potential temperature between 10°N–10°S at the lapse rate tropopause (PPT10mean, yellow) and at the cold point (PPTcp10mean, purple) as well as the 380 K isentrope. Solid lines show the mean trends, the shading denotes the associated standard deviation for the respective surface. Colored shading marks regions with trends of at least 95 % significance. Regions with grey shading are considered to show statistically insignificant trends. Note that the pressure trend axis is inverted because decreasing pressure implies an upward trend.

For comparison, the intersections of the 2 PVU and lapse rate tropopause with isentropes between 330–370 K are determined in addition. The 380 K isentrope often does not intersect with the respective tropopause, which is why it is not further considered. The zonal mean latitudes of the intersection between the lapse rate (2 PVU) tropopause and the 350 K isentrope, i.e. the lateral LMS boundaries in this study, vary between 29°N–48°N (26°N–40°N) and 31°S–45 S (26°S–36°S), with the lapse rate tropopause intersection always poleward of the 2 PVU intersection. Other definitions of the lateral LMS boundaries have been used in the literature like the intersection between the respective upper and lower LMS boundary surfaces (Appenzeller et al., 1996; Hegglin et al., 2010) or the zero diabatic heating rate at the upper LMS boundary surface (Wang and Fu, 2021; Wang et al., 2022). We consider the latitude of the intersection between tropopause and the 350 K isentrope to be a practical approximation of the location of the physical transport barrier between the (extratropical) LMS and the tropical troposphere, marked by the isentropic PV-gradient tropopause.

Beside the seasonal variability, the DLM identifies a trend of the intersections between tropopause and 350 K isentrope (Fig. 9). Here, the intersections of the zonal mean tropopause and isentropes are considered. In the NH, this trend is directed poleward for the lapse rate tropopause as well as 2 PVU. Such a poleward tendency is also evident for intersections of the NH tropopause with isentropes at 360 K and 370 K, which indicates an expansion of the NH tropics. This is consistent with evidence for a widening of the tropical belt, reported in many studies (Birner, 2010a; Wilcox et al., 2012a; Xian and Homeyer,

https://doi.org/10.5194/egusphere-2024-1700
Preprint. Discussion started: 13 June 2024
© Author(s) 2024. CC BY 4.0 License.

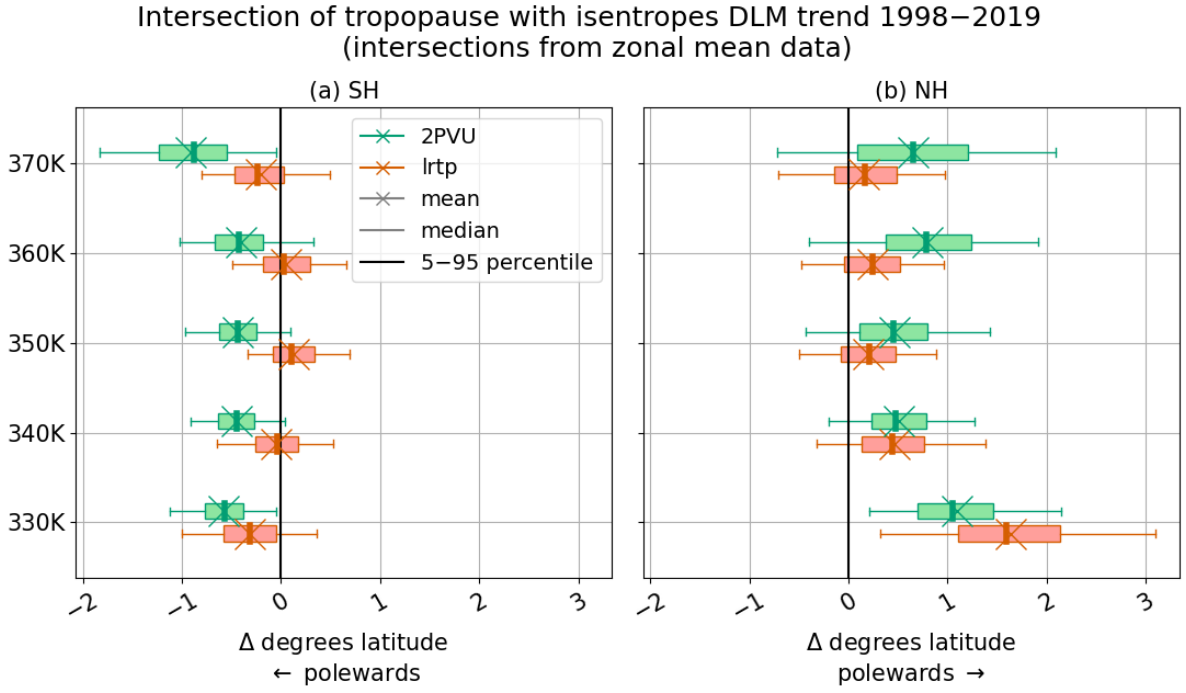

Figure 9. Trend of lateral intersections of the lapse rate tropopause (red, lower boxes) and the 2 PVU tropopause (green, upper boxes) with isentropes between 330–370 K (y-axis). The trends are DLM estimates for the time period 1998–2019. In the SH (a), negative trends are associated with a poleward tendency, in the NH (b), positive trends indicate a poleward shift. The DLM trend estimates are presented as box-whisker plots.

285 2019, e.g.,).

In the SH, on the other hand, the intersection between the lapse rate tropopause and 350 K shows an equatorward tendency while the trend of the intersection with the 2 PVU surface is directed poleward. At 330 K and 370 K, both tropopauses show a poleward tendency in the SH as well. A similar shape of lateral tropopause trends with respect to potential temperature has been found for the PV-gradient tropopause by Turhal et al. (2024). The different magnitudes of the lateral trends for tropopause
290 intersections with different isentropes suggests a shape change of the tropopause break. The larger poleward tendency of the tropopause around 370 K hints at a steeper tropopause. This could be associated with higher zonal wind speeds, i.e. an intensification of the subtropical jet (Manney and Hegglin, 2018; Maher et al., 2020). Furthermore, such a steepening of the tropopause break could be an indication of a strengthened BDC (Birner, 2010b).

As far as the LMS mass is concerned, the temporal evolution of the lower, upper and lateral LMS boundaries points towards a
295 trend of the LMS mass, which will be addressed in Sect. 3.3.3.

https://doi.org/10.5194/egusphere-2024-1700
Preprint. Discussion started: 13 June 2024
© Author(s) 2024. CC BY 4.0 License.

3.3.2 LMS mass climatology

The average global LMS mass between the different boundary surfaces ranges from $0.99 \pm 0.28 \cdot 10^{17}$ kg (lrtp-PPT10mean) to $1.89 \pm 0.37 \cdot 10^{17}$ kg (2 PVU-PPTcp10mean) within the time period 1979–2019. Since the 2 PVU tropopause is located at higher pressure than the lapse rate tropopause, the LMS mass between 2 PVU and the respective upper boundary is always larger than the mass with respect to the thermal tropopause. The fact that the LMS mass with respect to the 2 PVU tropopause exceeds the mass with respect to the thermal tropopause by a factor of 1.6–1.8 highlights that lower layers contribute disproportionately more mass due to the exponential decrease of density with height. Accordingly, the LMS mass with respect to the different upper boundary surfaces varies by less than 15 % for the same lower boundary and hemisphere. The mean LMS mass between all considered boundary surfaces on both hemispheres is listed in Tab. 1.

study and data	LMS	NH	SH
this study:			
ERA5	lrtp-PPT10mean	0.49±0.20	0.50±0.08
	lrtp-PPTcp10mean	0.56±0.22	0.58±0.09
	lrtp-380K	0.55±0.20	0.57±0.10
	2PVU-PPT10mean	0.80±0.24	0.90±0.11
	2PVU-PPTcp10mean	0.89±0.25	1.00±0.12
	2PVU-380K	0.88±0.23	0.99±0.13
Appenzeller et al. (1996):			
UKMO	2 PVU–380 K	2.3±0.4	2.4±0.1
Hegglin et al. (2010):			
NCEP	lrtp–100 hPa	1.6±0.3	1.5±0.1

Table 1. Mean LMS mass and associated standard deviation in 10^{17} kg for different LMS definitions and data. In this study, monthly LMS mass data is averaged over 1979–2019 and rounded to the second decimal. In Appenzeller et al. (1996) Fig. 5, daily LMS mass values from UKMO data are presented for the years 1992 and 1993. Fig. 6 in Hegglin et al. (2010) shows monthly mean LMS mass from NCEP data averaged over the time period 1990–1999. The LMS mass values from Appenzeller et al. (1996) and Hegglin et al. (2010) in this table are estimated from the respective figures.

The NH mean LMS mass is smaller than the SH mass, independent of the boundary surfaces. This is due to the greater seasonal variability of the LMS mass in the NH, reaching smaller minima in summer than in the SH. Within one hemisphere, low latitudes contribute considerably more to the LMS mass than high latitudes due to the area decrease from equator to pole.

The LMS mass calculated from ERA5 data between the respective boundary surfaces can be compared to results reported by Appenzeller et al. (1996) and Hegglin et al. (2010) (Tab. 1). On average, the LMS mass from ERA5 (this study) is 1.5 to 4.8 times smaller than previously reported. Reason for the discrepancies are the choice of the boundaries and the different reanalysis data sets. ERA5, as used in this study, has the finest resolution with a horizontal grid spacing of 0.25° by 0.25°

https://doi.org/10.5194/egusphere-2024-1700
Preprint. Discussion started: 13 June 2024
© Author(s) 2024. CC BY 4.0 License.

and a vertical spacing of about 25–50 hPa in the UTLS. Appenzeller et al. (1996) integrate the pressure between the 2 PVU surface and the 380 K isentrope from UKMO (United Kingdom Meteorological Office) data with a horizontal grid of 2.5° latitude by 3.75° longitude and 50 hPa in the vertical, with zonal mean daily data for the year 1993. The resulting UKMO dynamic tropopause is situated around 50–100 hPa lower than the ERA5 2 PVU surface. Hegglin et al. (2010) use NCEP (National Centers for Environmental Prediction) monthly mean, zonal mean reanalysis data for the time period 1990–1999 with a horizontal grid of 2.5° by 2.5°. They choose the thermal tropopause as the lower and the 100 hPa isobar as a fixed upper boundary for the mass computation. The upper boundaries used in this study are (on average) situated between 90–187 hPa. For the lateral boundaries, Hegglin et al. (2010) and Appenzeller et al. (1996) use the intersections between upper and lower boundary surfaces. The lateral LMS boundaries in this study are at considerably higher latitudes. Using the same LMS boundary definitions as Hegglin et al. (2010) from ERA5 zonal mean data for the time period 1979–2019, we compute an average LMS mass of around $1 \cdot 10^{17}$ kg for each hemisphere. With a downward shift of the 2 PVU surface by 60 hPa, we obtain the same LMS mass as Appenzeller et al. (1996).

3.3.3 LMS mass trends

The trends of the LMS lower, upper and lateral boundaries presented in Sect. 3.1 and 3.3.1 suggest a long term change of the LMS mass enclosed by the respective boundary surfaces. The observed extratropical tropopause trends (Sect. 3.1, Fig. 2) and the lifting trend of the tropical tropopause (Fig. 7 and 8) indicate that the rise of the upper LMS boundary could potentially compensate for the rising lower boundary and the poleward transition of the lateral boundary. The results illustrated in Fig. 10a, b and d confirm this expectation. For the LMS bounded with 380 K, the DLM analysis results in a statistically significant negative trend of the LMS mass between 1998–2019 (except for the LMS mass with respect to SH lapse rate tropopause). In contrast, the LMS defined with a dynamical upper boundary based on the tropical tropopause (PPT10mean and PPTcp10mean) shows mean mass trends close to zero or even positive trends. Focusing on the latitude bins poleward of the mean lateral LMS boundary (latitude bins 50°–80° and 60°–90°), LMS mass changes are positive or smaller negative but stay significantly negative if 380 K is used as the upper boundary. This shows three things: 1) The decreasing NH LMS mass for a fixed 380 K boundary is largely due to the rising NH extratropical tropopause. 2) A considerable proportion of this NH LMS mass decline can be attributed to the poleward trend of the lateral boundary which is the result of an expansion of the tropics. 3) The "dynamical" upper boundary surfaces based on the tropical tropopause are indeed able to largely compensate for the tropopause rise, despite the density effect.

The SH LMS mass with respect to the lapse rate tropopause stands out with a significant LMS mass increase, regardless of the choice of the upper boundary (Fig. 10c). This is due to the downward trend of the SH extratropical lapse rate tropopause (Fig. 2a). Moreover, the intersection of the SH lapse rate tropopause with 350 K, which serves as the lateral LMS boundary, shows a small equatorward tendency (Fig. 9a). Interesting are for example the respective LMS mass trends between 40°S–70°S. Since the lapse rate tropopause change is close to zero between 40°S–70°S (Fig. 2a), the greater mass change for the SH LMS bounded with PPT10mean and PPTcp10mean compared to 380 K highlights the impact of the upper boundary surface.

https://doi.org/10.5194/egusphere-2024-1700
Preprint. Discussion started: 13 June 2024
© Author(s) 2024. CC BY 4.0 License.

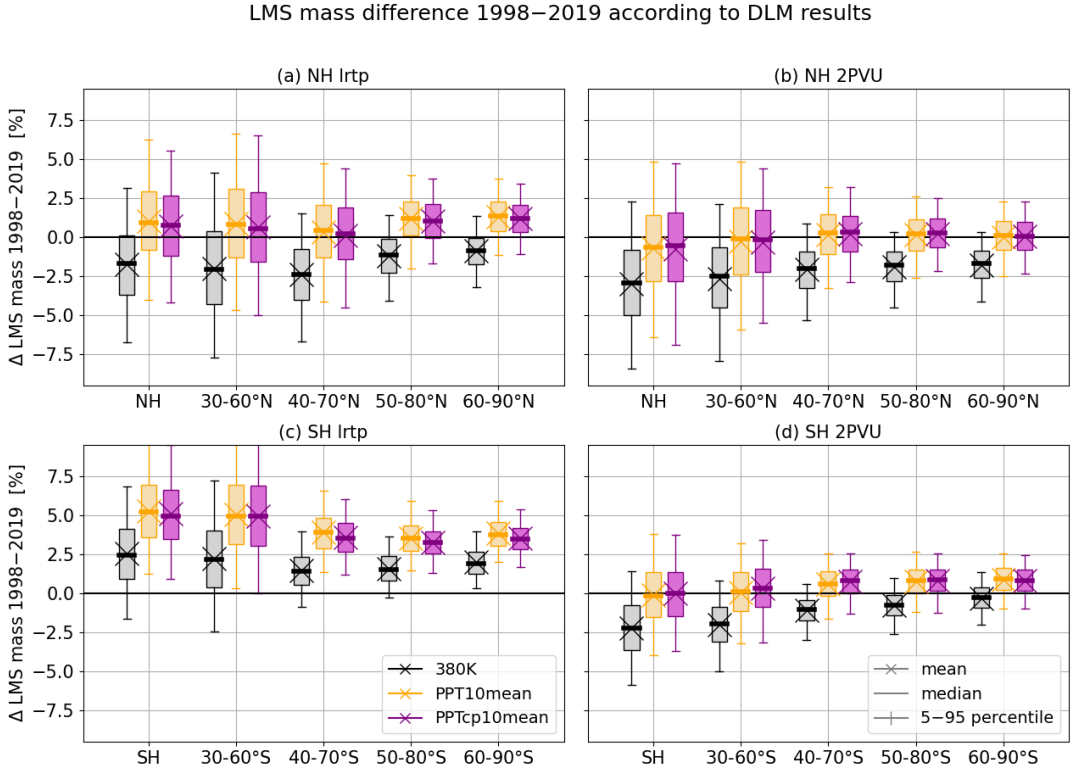

Figure 10. LMS mass change between 1998–2019 as estimated by the DLM. The DLM trend state differences are presented as box-whisker plots. The LMS mass has been analyzed for different latitude bins (x-axis) for both hemispheres (upper and lower panels). Moreover, different boundary surfaces have been compared. Panel (a) and (c) show the results for the LMS defined with the lapse rate tropopause as the lower boundary. In panel (b) and (d), the 2 PVU tropopause serves as the lower LMS edge. The results for the different upper boundary surfaces can be distinguished by the color of the box-whisker plots (380 K: black, PPT10mean: yellow, PPTcp10mean: purple).

4 Conclusions

In this study, we have analyzed long-term trends in the thermodynamic structure of the lowermost stratosphere based on ERA5 data for the period 1979–2019. Our DLM trend analysis shows that the zonal mean NH mid-latitude lapse rate tropopause as well as the 2 PVU surface are rising at a mean rate of about $-1\,\mathrm{hPa/decade}$ between 1998–2019, although the trends are hardly statistically significant. In the tropics and subtropics, the lapse rate tropopause and the cold point show a statistically significant upward trend of about $-0.5\,\mathrm{hPa/decade}$ and $-0.7\,\mathrm{hPa/decade}$, respectively, for the same time period. Consistent with the negative pressure trends, tropopause potential temperatures are increasing. These tropopause trends agree well with trends reported from different reanalyses (e.g., Wilcox et al., 2012a; Xian and Homeyer, 2019) and observational data (e.g., Meng et al., 2021). The tendency of the SH tropopause in this study is less clear. The SH lapse rate tropopause shows a down-

https://doi.org/10.5194/egusphere-2024-1700
Preprint. Discussion started: 13 June 2024
© Author(s) 2024. CC BY 4.0 License.

ward tendency ranging between 0 and +2 $\mathrm{hPa/decade}$ while the 2 PVU surface is rising at a mean rate of $-1\,\mathrm{hPa/decade}$. This positive pressure trend of the SH extratropical lapse rate tropopause agrees with the trends found by Xian and Homeyer (2019) for the JRA-55, MERRA-2 and CFSR reanalyses. However, it seems to contradict the results reported for ERA-Interim in the same study and by Wilcox et al. (2012a). Interestingly, our non-linear DLM trend analysis of the time series 1979–2019 reveals a trend reversal of the lapse rate tropopause around the year 2000. Accordingly, our results suggest an upward tendency of the SH mid-latitude lapse rate tropopause before the year 2000 and a downward tendency thereafter. This could be consistent with expected effects of ozone recovery and an accelerating BDC in the SH on tropopause height (Birner, 2010b). An acceleration of the BDC in the SH after about the year 2000 has also been estimated from age of air and long-lived trace gas measurements (Strahan et al., 2020; Ploeger and Garny, 2022).

The lateral positions of the intersections between the NH tropopause (lrtp as well as 2PVU) and isentropes between 330–370 K show a poleward shift after 1998. This can be associated with a widening of the tropics in the NH, which has been reported in many studies (e.g., Seidel and Randel, 2007; Meng et al., 2021; Wilcox et al., 2012a; Grise et al., 2019; Staten et al., 2018). For the SH, the lateral trends of the intersections between lapse rate tropopause and 350 K are directed equatorwards while 330 K and 370 K show a poleward tendency. The different magnitude of the lateral trends with respect to the potential temperature on both hemispheres and both tropopause definitions suggests a steepening of the tropopause break. A similar shape of lateral tropopause trends with respect to potential temperature has been found for the PV-gradient tropopause by Turhal et al. (2024). Such a steepening of the tropopause break can be associated with an intensification of the SH subtropical jet (Manney and Hegglin, 2018; Maher et al., 2020) and could be linked to a strengthening of the BDC (Birner, 2010b).

Since the NH tropopause is rising and expanding towards the poles, the mass of the lowermost stratosphere (LMS) can be expected to decrease if the upper boundary is fixed. However, as the upper LMS boundary is properly defined by the tropical tropopause, which is also rising, the negative LMS mass trends disappear when using this dynamic upper boundary in the calculation. According to this study, the NH LMS mass trend for the period 1998–2019 changes from around $-2\,\%$ for the LMS upper boundary defined by 380 K to around +1 $\%$ for an LMS upper boundary defined with respect to the lapse rate tropopause. The LMS mass trend with respect to the 2 PVU isosurface stays negative but close to zero with dynamical upper boundaries. Even though pressure trends at the upper and lower boundary are comparable, the lower boundary dominates LMS mass changes owing to the exponential density decrease with altitude. Furthermore, a poleward expansion of the tropical troposphere can substantially decrease LMS mass due to the area decrease from low to high latitudes.

LMS mass changes are important to consider because the LMS mass makes up about 20 $\%$ of the stratospheric column and therefore contains a substantial fraction of, for example, column ozone. Since the interannual ozone variability in the LMS is mainly controlled by dynamics (e.g., Chipperfield et al., 2018), ozone changes are expected to be directly related to LMS mass changes. LMS ozone changes do not only have important implications on the radiative budget in the lower stratosphere but also on atmospheric chemistry and the UV radiation reaching the surface (e.g., Forster and Shine, 1997; Hegglin and Shepherd, 2009).

https://doi.org/10.5194/egusphere-2024-1700
Preprint. Discussion started: 13 June 2024
© Author(s) 2024. CC BY 4.0 License.

Code and data availability. ERA5 reanalysis data are available from the European Centre for Medium-range Weather Forecasts (https://apps.ecmwf.int/data-catalogues/era5/?class=ea, ECMWF, 2024). The DLM model code (dlmmc) is publicly available at https://github.com/justinalsing/dlmmc. LMS mass data and the code for LMS mass calculation, including the respective LMS boundary surfaces, is available on request to the authors.

Author contributions. FW performed the analyses and wrote the first draft of the paper. PH and DK initiated the project and conceptualized the core research goals. FP and TB contributed valuable ideas. KT provided the PV-gradient tropopause data. All authors contributed in interpreting the results and improving the manuscript.

Competing interests. The authors declare that they have no conflict of interest.

Acknowledgements. This work was funded by the Deutsche Forschungsgemeinschaft (DFG, German Research Foundation) – TRR 301 – Project-ID 428312742: "The tropopause region in a changing atmosphere". We further would like to thank the Dres. Göbel Klima-Stiftung for their financial support, which FW was able to benefit from as part of a Deutschlandstipendium during her Master's programme.

https://doi.org/10.5194/egusphere-2024-1700
Preprint. Discussion started: 13 June 2024
© Author(s) 2024. CC BY 4.0 License.

References

Alsing, J.: dlmmc: Dynamical linear model regression for atmospheric time-series analysis, Journal of Open Source Software, 4, 1157, https://doi.org/10.21105/joss.01157, 2019.

Appenzeller, C., Holton, J. R., and Rosenlof, K. H.: Seasonal variation of mass transport across the tropopause, Journal of Geophysical Research: Atmospheres, 101, 15 071–15 078, https://doi.org/10.1029/96JD00821, 1996.

Ball, W. T., Alsing, J., Mortlock, D. J., Rozanov, E. V., Tummon, F., and Haigh, J. D.: Reconciling differences in stratospheric ozone composites, Atmospheric Chemistry and Physics, 17, 12 269–12 302, https://doi.org/10.5194/acp-17-12269-2017, 2017.

Ball, W. T., Alsing, J., Mortlock, D. J., Staehelin, J., Haigh, J. D., Peter, T., Tummon, F., Stübi, R., Stenke, A., Anderson, J., Bourassa, A., Davis, S. M., Degenstein, D., Frith, S., Froidevaux, L., Roth, C., Sofieva, V., Wang, R., Wild, J., Yu, P., Ziemke, J. R., and Rozanov, E. V.: Evidence for a continuous decline in lower stratospheric ozone offsetting ozone layer recovery, Atmospheric Chemistry and Physics, 18, 1379–1394, https://doi.org/10.5194/acp-18-1379-2018, 2018.

Ball, W. T., Alsing, J., Staehelin, J., Davis, S. M., Froidevaux, L., and Peter, T.: Stratospheric ozone trends for 1985-2018: sensitivity to recent large variability, preprint, Gases/Remote Sensing/Stratosphere/Physics (physical properties and processes), https://doi.org/10.5194/acp-2019-243, 2019.

Berthet, G., Esler, J. G., and Haynes, P. H.: A Lagrangian perspective of the tropopause and the ventilation of the lowermost stratosphere, Journal of Geophysical Research: Atmospheres, 112, 2006JD008 295, https://doi.org/10.1029/2006JD008295, 2007.

Bethan, S., Vaughan, G., and Reid, S. J.: A comparison of ozone and thermal tropopause heights and the impact of tropopause definition on quantifying the ozone content of the troposphere, Quarterly Journal of the Royal Meteorological Society, 122, 929–944, https://doi.org/10.1002/qj.49712253207, 1996.

Birner, T.: Fine-scale structure of the extratropical tropopause region, Journal of Geophysical Research: Atmospheres, 111, 2005JD006 301, https://doi.org/10.1029/2005JD006301, 2006.

Birner, T.: Recent widening of the tropical belt from global tropopause statistics: Sensitivities, Journal of Geophysical Research: Atmospheres, 115, 2010JD014 664, https://doi.org/10.1029/2010JD014664, 2010a.

Birner, T.: Residual Circulation and Tropopause Structure, Journal of the Atmospheric Sciences, 67, 2582–2600, https://doi.org/10.1175/2010JAS3287.1, 2010b.

Birner, T., Dörnbrack, A., and Schumann, U.: How sharp is the tropopause at midlatitudes?, Geophysical Research Letters, 29, https://doi.org/10.1029/2002GL015142, 2002.

Bognar, K., Tegtmeier, S., Bourassa, A., Roth, C., Warnock, T., Zawada, D., and Degenstein, D.: Stratospheric ozone trends for 1984–2021 in the SAGE II–OSIRIS–SAGE III/ISS composite dataset, Atmospheric Chemistry and Physics, 22, 9553–9569, https://doi.org/10.5194/acp-22-9553-2022, 2022.

Boljka, L. and Birner, T.: Potential impact of tropopause sharpness on the structure and strength of the general circulation, npj Climate and Atmospheric Science, 5, 98, https://doi.org/10.1038/s41612-022-00319-6, 2022.

Butchart, N.: The Brewer-Dobson circulation, Reviews of Geophysics, 52, 157–184, https://doi.org/10.1002/2013RG000448, 2014.

Charlesworth, E., Plöger, F., Birner, T., Baikhadzhaev, R., Abalos, M., Abraham, N. L., Akiyoshi, H., Bekki, S., Dennison, F., Jöckel, P., Keeble, J., Kinnison, D., Morgenstern, O., Plummer, D., Rozanov, E., Strode, S., Zeng, G., Egorova, T., and Riese, M.: Stratospheric water vapor affecting atmospheric circulation, Nature Communications, 14, 3925, https://doi.org/10.1038/s41467-023-39559-2, 2023.

https://doi.org/10.5194/egusphere-2024-1700
Preprint. Discussion started: 13 June 2024
© Author(s) 2024. CC BY 4.0 License.

Chipperfield, M. P., Dhomse, S., Hossaini, R., Feng, W., Santee, M. L., Weber, M., Burrows, J. P., Wild, J. D., Loyola, D., and Coldewey-Egbers, M.: On the Cause of Recent Variations in Lower Stratospheric Ozone, Geophysical Research Letters, 45, 5718–5726, https://doi.org/10.1029/2018GL078071, 2018.

ECMWF: ERA5 reanalysis, https://apps.ecmwf.int/data-catalogues/era5/?class=ea, last accessed: 29 May 2024.

ECMWF: IFS Documentation CY41R2 - Part VI: Technical and Computational Procedures, https://doi.org/10.21957/5RWD87QEW, publisher: [object Object], 2016.

Fischer, H., Wienhold, F. G., Hoor, P., Bujok, O., Schiller, C., Siegmund, P., Ambaum, M., Scheeren, H. A., and Lelieveld, J.: Tracer correlations in the northern high latitude lowermost stratosphere: Influence of cross-tropopause mass exchange, Geophysical Research Letters, 27, 97–100, https://doi.org/10.1029/1999GL010879, 2000.

Forster, F., P. M. and Shine, K. P.: Radiative forcing and temperature trends from stratospheric ozone changes, Journal of Geophysical Research: Atmospheres, 102, 10 841–10 855, https://doi.org/10.1029/96JD03510, 1997.

Forster, P. M. D. F. and Shine, K. P.: Assessing the climate impact of trends in stratospheric water vapor, Geophysical Research Letters, 29, https://doi.org/10.1029/2001GL013909, 2002.

Fu, Q., Solomon, S., Pahlavan, H. A., and Lin, P.: Observed changes in Brewer–Dobson circulation for 1980–2018, Environmental Research Letters, 14, 114 026, https://doi.org/10.1088/1748-9326/ab4de7, 2019.

FU-Berlin: The Quasi-Biennial oscillation (QBO) Data Serie, https://www.geo.fu-berlin.de/met/ag/strat/produkte/qbo/qbo.dat, last accessed: 11 July 2023.

Gettelman, A. and Wang, T.: Structural diagnostics of the tropopause inversion layer and its evolution, Journal of Geophysical Research: Atmospheres, 120, 46–62, https://doi.org/10.1002/2014JD021846, 2015.

Gettelman, A., Hegglin, M. I., Son, S.-W., Kim, J., Fujiwara, M., Birner, T., Kremser, S., Rex, M., Añel, J. A., Akiyoshi, H., Austin, J., Bekki, S., Braesike, P., Brühl, C., Butchart, N., Chipperfield, M., Dameris, M., Dhomse, S., Garny, H., Hardiman, S. C., Jöckel, P., Kinnison, D. E., Lamarque, J. F., Mancini, E., Marchand, M., Michou, M., Morgenstern, O., Pawson, S., Pitari, G., Plummer, D., Pyle, J. A., Rozanov, E., Scinocca, J., Shepherd, T. G., Shibata, K., Smale, D., Teyssèdre, H., and Tian, W.: Multimodel assessment of the upper troposphere and lower stratosphere: Tropics and global trends, Journal of Geophysical Research, 115, D00M08, https://doi.org/10.1029/2009JD013638, 2010.

Gettelman, A., Hoor, P., Pan, L. L., Randel, W. J., Hegglin, M. I., and Birner, T.: The Extratropical Upper Troposphere and Lower Stratosphere, Reviews of Geophysics, 49, RG3003, https://doi.org/10.1029/2011RG000355, 2011.

Grise, K. M., Davis, S. M., Simpson, I. R., Waugh, D. W., Fu, Q., Allen, R. J., Rosenlof, K. H., Ummenhofer, C. C., Karnauskas, K. B., Maycock, A. C., Quan, X.-W., Birner, T., and Staten, P. W.: Recent Tropical Expansion: Natural Variability or Forced Response?, Journal of Climate, 32, 1551–1571, https://doi.org/10.1175/JCLI-D-18-0444.1, 2019.

Hegglin, M. I. and Shepherd, T. G.: Large climate-induced changes in ultraviolet index and stratosphere-to-troposphere ozone flux, Nature Geoscience, 2, 687–691, https://doi.org/10.1038/ngeo604, 2009.

Hegglin, M. I., Gettelman, A., Hoor, P., Krichevsky, R., Manney, G. L., Pan, L. L., Son, S.-W., Stiller, G., Tilmes, S., Walker, K. A., Eyring, V., Shepherd, T. G., Waugh, D., Akiyoshi, H., Añel, J. A., Austin, J., Baumgaertner, A., Bekki, S., Braesicke, P., Brühl, C., Butchart, N., Chipperfield, M., Dameris, M., Dhomse, S., Frith, S., Garny, H., Hardiman, S. C., Jöckel, P., Kinnison, D. E., Lamarque, J. F., Mancini, E., Michou, M., Morgenstern, O., Nakamura, T., Olivié, D., Pawson, S., Pitari, G., Plummer, D. A., Pyle, J. A., Rozanov, E., Scinocca, J. F., Shibata, K., Smale, D., Teyssèdre, H., Tian, W., and Yamashita, Y.: Multimodel assessment of the upper troposphere and lower stratosphere: Extratropics, Journal of Geophysical Research, 115, D00M09, https://doi.org/10.1029/2010JD013884, 2010.

https://doi.org/10.5194/egusphere-2024-1700
Preprint. Discussion started: 13 June 2024
© Author(s) 2024. CC BY 4.0 License.

Hersbach, H., Bell, B., Berrisford, P., Hirahara, S., Horányi, A., Muñoz-Sabater, J., Nicolas, J., Peubey, C., Radu, R., Schepers, D., Simmons, A., Soci, C., Abdalla, S., Abellan, X., Balsamo, G., Bechtold, P., Biavati, G., Bidlot, J., Bonavita, M., Chiara, G., Dahlgren, P., Dee, D., Diamantakis, M., Dragani, R., Flemming, J., Forbes, R., Fuentes, M., Geer, A., Haimberger, L., Healy, S., Hogan, R. J., Hólm, E., Janisková, M., Keeley, S., Laloyaux, P., Lopez, P., Lupu, C., Radnoti, G., Rosnay, P., Rozum, I., Vamborg, F., Villaume, S., and Thépaut, J.: The ERA5 global reanalysis, Quarterly Journal of the Royal Meteorological Society, p. qj.3803, https://doi.org/10.1002/qj.3803, 2020.

Hoerling, M., Schaack, T., and Lenzen, A.: Global objective tropopause analysis, pp. 1816–1831, 1991.

Holton, J. R., Haynes, P. H., McIntyre, M. E., Douglass, A. R., Rood, R. B., and Pfister, L.: Stratosphere-troposphere exchange, Reviews of Geophysics, 33, 403, https://doi.org/10.1029/95RG02097, 1995.

Hoor, P., Fischer, H., Lange, L., Lelieveld, J., and Brunner, D.: Seasonal variations of a mixing layer in the lowermost stratosphere as identified by the CO-O $_3$ correlation from in situ measurements, Journal of Geophysical Research: Atmospheres, 107, https://doi.org/10.1029/2000JD000289, 2002.

Hoor, P., Gurk, C., Brunner, D., Hegglin, M. I., Wernli, H., and Fischer, H.: Seasonality and extent of extratropical TST derived from in-situ CO measurements during SPURT, Atmospheric Chemistry and Physics, 4, 1427–1442, https://doi.org/10.5194/acp-4-1427-2004, 2004.

Hoskins, B. J.: Towards a PV-theta view of the general circulation, Tellus A, 43, 27–35, https://doi.org/10.1034/j.1600-0870.1991.t01-3-00005.x, 1991.

IPCC, Calvin, K., Dasgupta, D., Krinner, G., Mukherji, A., Thorne, P. W., Trisos, C., Romero, J., Aldunce, P., Barrett, K., Blanco, G., Cheung, W. W., Connors, S., Denton, F., Diongue-Niang, A., Dodman, D., Garschagen, M., Geden, O., Hayward, B., Jones, C., Jotzo, F., Krug, T., Lasco, R., Lee, Y.-Y., Masson-Delmotte, V., Meinshausen, M., Mintenbeck, K., Mokssit, A., Otto, F. E., Pathak, M., Pirani, A., Poloczanska, E., Pörtner, H.-O., Revi, A., Roberts, D. C., Roy, J., Ruane, A. C., Skea, J., Shukla, P. R., Slade, R., Slangen, A., Sokona, Y., Sörensson, A. A., Tignor, M., Van Vuuren, D., Wei, Y.-M., Winkler, H., Zhai, P., Zommers, Z., Hourcade, J.-C., Johnson, F. X., Pachauri, S., Simpson, N. P., Singh, C., Thomas, A., Totin, E., Arias, P., Bustamante, M., Elgizouli, I., Flato, G., Howden, M., Méndez-Vallejo, C., Pereira, J. J., Pichs-Madruga, R., Rose, S. K., Saheb, Y., Sánchez Rodríguez, R., Ürge Vorsatz, D., Xiao, C., Yassaa, N., Alegría, A., Armour, K., Bednar-Friedl, B., Blok, K., Cissé, G., Dentener, F., Eriksen, S., Fischer, E., Garner, G., Guivarch, C., Haasnoot, M., Hansen, G., Hauser, M., Hawkins, E., Hermans, T., Kopp, R., Leprince-Ringuet, N., Lewis, J., Ley, D., Ludden, C., Niamir, L., Nicholls, Z., Some, S., Szopa, S., Trewin, B., Van Der Wijst, K.-I., Winter, G., Witting, M., Birt, A., Ha, M., Romero, J., Kim, J., Haites, E. F., Jung, Y., Stavins, R., Birt, A., Ha, M., Orendain, D. J. A., Ignon, L., Park, S., Park, Y., Reisinger, A., Cammaramo, D., Fischlin, A., Fuglestvedt, J. S., Hansen, G., Ludden, C., Masson-Delmotte, V., Matthews, J. R., Mintenbeck, K., Pirani, A., Poloczanska, E., Leprince-Ringuet, N., and Péan, C.: IPCC, 2023: Climate Change 2023: Synthesis Report. Contribution of Working Groups I, II and III to the Sixth Assessment Report of the Intergovernmental Panel on Climate Change [Core Writing Team, H. Lee and J. Romero (eds.)]. IPCC, Geneva, Switzerland., Tech. rep., Intergovernmental Panel on Climate Change (IPCC), https://doi.org/10.59327/IPCC/AR6-9789291691647, edition: First, 2023.

Kaluza, T., Kunkel, D., and Hoor, P.: On the occurrence of strong vertical wind shear in the tropopause region: a 10-year ERA5 northern hemispheric study, Weather and Climate Dynamics, 2, 631–651, https://doi.org/10.5194/wcd-2-631-2021, 2021.

Karagodin-Doyennel, A., Rozanov, E., Sukhodolov, T., Egorova, T., Sedlacek, J., Ball, W., and Peter, T.: The historical ozone trends simulated with the SOCOLv4 and their comparison with observations and reanalyses, Atmospheric Chemistry and Physics, 22, 15 333–15 350, https://doi.org/10.5194/acp-22-15333-2022, 2022.

Kunkel, D., Hoor, P., Kaluza, T., Ungermann, J., Kluschat, B., Giez, A., Lachnitt, H.-C., Kaufmann, M., and Riese, M.: Evidence of small-scale quasi-isentropic mixing in ridges of extratropical baroclinic waves, Atmospheric Chemistry and Physics, 19, 12 607–12 630, https://doi.org/10.5194/acp-19-12607-2019, 2019.

https://doi.org/10.5194/egusphere-2024-1700
Preprint. Discussion started: 13 June 2024
© Author(s) 2024. CC BY 4.0 License.

Kunz, A., Konopka, P., Müller, R., and Pan, L. L.: Dynamical tropopause based on isentropic potential vorticity gradients, Journal of Geophysical Research, 116, D01 110, https://doi.org/10.1029/2010JD014343, 2011.

Laine, M., Latva-Pukkila, N., and Kyrölä, E.: Analysing time-varying trends in stratospheric ozone time series using the state space approach, Atmospheric Chemistry and Physics, 14, 9707–9725, https://doi.org/10.5194/acp-14-9707-2014, 2014.

Lu, J., Deser, C., and Reichler, T.: Cause of the widening of the tropical belt since 1958, Geophysical Research Letters, 36, 2008GL036 076, https://doi.org/10.1029/2008GL036076, 2009.

Maher, P., Kelleher, M. E., Sansom, P. G., and Methven, J.: Is the subtropical jet shifting poleward?, Climate Dynamics, 54, 1741–1759, https://doi.org/10.1007/s00382-019-05084-6, 2020.

Manney, G. L. and Hegglin, M. I.: Seasonal and Regional Variations of Long-Term Changes in Upper-Tropospheric Jets from Reanalyses, Journal of Climate, 31, 423–448, https://doi.org/10.1175/JCLI-D-17-0303.1, 2018.

Manney, G. L., Hegglin, M. I., Daffer, W. H., Santee, M. L., Ray, E. A., Pawson, S., Schwartz, M. J., Boone, C. D., Froidevaux, L., Livesey, N. J., Read, W. G., and Walker, K. A.: Jet characterization in the upper troposphere/lower stratosphere (UTLS): applications to climatology and transport studies, Atmospheric Chemistry and Physics, 11, 6115–6137, https://doi.org/10.5194/acp-11-6115-2011, 2011.

Meng, L., Liu, J., Tarasick, D. W., Randel, W. J., Steiner, A. K., Wilhelmsen, H., Wang, L., and Haimberger, L.: Continuous rise of the tropopause in the Northern Hemisphere over 1980–2020, Science Advances, 7, eabi8065, https://doi.org/10.1126/sciadv.abi8065, 2021.

NOAA: Multivariate ENSO Index Version 2 (MEI.v2), https://psl.noaa.gov/enso/mei/, last accessed: 11 July 2023.

Olsen, M. A., Douglass, A. R., and Kaplan, T. B.: Variability of extratropical ozone stratosphere–troposphere exchange using microwave limb sounder observations, Journal of Geophysical Research: Atmospheres, 118, 1090–1099, https://doi.org/10.1029/2012JD018465, 2013.

Pan, L. L., Randel, W. J., Gary, B. L., Mahoney, M. J., and Hintsa, E. J.: Definitions and sharpness of the extratropical tropopause: A trace gas perspective, Journal of Geophysical Research: Atmospheres, 109, 2004JD004 982, https://doi.org/10.1029/2004JD004982, 2004.

Pisoft, P., Sacha, P., Polvani, L. M., Añel, J. A., De La Torre, L., Eichinger, R., Foelsche, U., Huszar, P., Jacobi, C., Karlicky, J., Kuchar, A., Miksovsky, J., Zak, M., and Rieder, H. E.: Stratospheric contraction caused by increasing greenhouse gases, Environmental Research Letters, 16, 064 038, https://doi.org/10.1088/1748-9326/abfe2b, 2021.

Ploeger, F. and Garny, H.: Hemispheric asymmetries in recent changes in the stratospheric circulation, Atmospheric Chemistry and Physics, 22, 5559–5576, https://doi.org/10.5194/acp-22-5559-2022, 2022.

Randel, W. J., Wu, F., and Forster, P.: The Extratropical Tropopause Inversion Layer: Global Observations with GPS Data, and a Radiative Forcing Mechanism, Journal of the Atmospheric Sciences, 64, 4489–4496, https://doi.org/10.1175/2007JAS2412.1, 2007.

Reichler, T., Dameris, M., and Sausen, R.: Determining the tropopause height from gridded data, Geophysical Research Letters, 30, 2003GL018 240, https://doi.org/10.1029/2003GL018240, 2003.

Riese, M., Ploeger, F., Rap, A., Vogel, B., Konopka, P., Dameris, M., and Forster, P.: Impact of uncertainties in atmospheric mixing on simulated UTLS composition and related radiative effects, Journal of Geophysical Research: Atmospheres, 117, n/a–n/a, https://doi.org/10.1029/2012JD017751, 2012.

Santer, B. D.: Behavior of tropopause height and atmospheric temperature in models, reanalyses, and observations: Decadal changes, Journal of Geophysical Research, 108, 4002, https://doi.org/10.1029/2002JD002258, 2003a.

Santer, B. D.: Contributions of Anthropogenic and Natural Forcing to Recent Tropopause Height Changes, Science, 301, 479–483, https://doi.org/10.1126/science.1084123, 2003b.

Santer, B. D., Wigley, T. M. L., Simmons, A. J., Kållberg, P. W., Kelly, G. A., Uppala, S. M., Ammann, C., Boyle, J. S., Brüggemann, W., Doutriaux, C., Fiorino, M., Mears, C., Meehl, G. A., Sausen, R., Taylor, K. E., Washington, W. M., Wehner, M. F., and Wentz, F. J.:

https://doi.org/10.5194/egusphere-2024-1700
Preprint. Discussion started: 13 June 2024
© Author(s) 2024. CC BY 4.0 License.

Identification of anthropogenic climate change using a second-generation reanalysis, Journal of Geophysical Research: Atmospheres, 109, n/a–n/a, https://doi.org/10.1029/2004JD005075, 2004.

Sausen, R. and Santer, B. D.: Use of changes in tropopause height to detect human influences on climate, Meteorologische Zeitschrift, 12, 131–136, https://doi.org/10.1127/0941-2948/2003/0012-0131, 2003.

Scherllin-Pirscher, B., Steiner, A. K., Anthes, R. A., Alexander, M. J., Alexander, S. P., Biondi, R., Birner, T., Kim, J., Randel, W. J., Son, S.-W., Tsuda, T., and Zeng, Z.: Tropical Temperature Variability in the UTLS: New Insights from GPS Radio Occultation Observations, Journal of Climate, 34, 2813–2838, https://doi.org/10.1175/JCLI-D-20-0385.1, 2021.

Schmidt, T., Wickert, J., Beyerle, G., and Heise, S.: Global tropopause height trends estimated from GPS radio occultation data, Geophysical Research Letters, 35, L11 806, https://doi.org/10.1029/2008GL034012, 2008.

Schoeberl, M. R.: Extratropical stratosphere-troposphere mass exchange, Journal of Geophysical Research: Atmospheres, 109, n/a–n/a, https://doi.org/10.1029/2004JD004525, 2004.

Seidel, D. J. and Randel, W. J.: Variability and trends in the global tropopause estimated from radiosonde data, Journal of Geophysical Research, 111, D21 101, https://doi.org/10.1029/2006JD007363, 2006.

Seidel, D. J. and Randel, W. J.: Recent widening of the tropical belt: Evidence from tropopause observations, Journal of Geophysical Research, 112, D20 113, https://doi.org/10.1029/2007JD008861, 2007.

Seidel, D. J., Ross, R. J., Angell, J. K., and Reid, G. C.: Climatological characteristics of the tropical tropopause as revealed by radiosondes, Journal of Geophysical Research: Atmospheres, 106, 7857–7878, https://doi.org/10.1029/2000JD900837, 2001.

Staten, P. W., Lu, J., Grise, K. M., Davis, S. M., and Birner, T.: Re-examining tropical expansion, Nature Climate Change, 8, 768–775, https://doi.org/10.1038/s41558-018-0246-2, 2018.

Stohl, A.: Stratosphere-troposphere exchange: A review, and what we have learned from STACCATO, Journal of Geophysical Research, 108, 8516, https://doi.org/10.1029/2002JD002490, 2003.

Strahan, S. E., Smale, D., Douglass, A. R., Blumenstock, T., Hannigan, J. W., Hase, F., Jones, N. B., Mahieu, E., Notholt, J., Oman, L. D., Ortega, I., Palm, M., Prignon, M., Robinson, J., Schneider, M., Sussmann, R., and Velazco, V. A.: Observed Hemispheric Asymmetry in Stratospheric Transport Trends From 1994 to 2018, Geophysical Research Letters, 47, https://doi.org/10.1029/2020GL088567, 2020.

Tegtmeier, S., Anstey, J., Davis, S., Dragani, R., Harada, Y., Ivanciu, I., Pilch Kedzierski, R., Krüger, K., Legras, B., Long, C., Wang, J. S., Wargan, K., and Wright, J. S.: Temperature and tropopause characteristics from reanalyses data in the tropical tropopause layer, Atmospheric Chemistry and Physics, 20, 753–770, https://doi.org/10.5194/acp-20-753-2020, 2020.

Thomason, L. W., Ernest, N., Millán, L., Rieger, L., Bourassa, A., Vernier, J.-P., Manney, G., Luo, B., Arfeuille, F., and Peter, T.: A global space-based stratospheric aerosol climatology: 1979–2016, Earth System Science Data, 10, 469–492, https://doi.org/10.5194/essd-10-469-2018, 2018.

Thompson, D. W. J. and Solomon, S.: Understanding Recent Stratospheric Climate Change, Journal of Climate, 22, 1934–1943, https://doi.org/10.1175/2008JCLI2482.1, 2009.

Tinney, E. N., Homeyer, C. R., Elizalde, L., Hurst, D. F., Thompson, A. M., Stauffer, R. M., Vömel, H., and Selkirk, H. B.: A Modern Approach to a Stability-Based Definition of the Tropopause, Monthly Weather Review, 150, 3151–3174, https://doi.org/10.1175/MWR-D-22-0174.1, 2022.

Turhal, K., Plöger, F., Clemens, J., Birner, T., Weyland, F., Konopka, P., and Hoor, P.: Variability and trends in the PV-gradient dynamical tropopause, https://doi.org/10.5194/egusphere-2024-471, 2024.

https://doi.org/10.5194/egusphere-2024-1700
Preprint. Discussion started: 13 June 2024
© Author(s) 2024. CC BY 4.0 License.

Wang, M. and Fu, Q.: Stratosphere-Troposphere Exchange of Air Masses and Ozone Concentrations Based on Reanalyses and Observations, Journal of Geophysical Research: Atmospheres, 126, https://doi.org/10.1029/2021JD035159, 2021.

Wang, M., Fu, Q., Solomon, S., Alexander, B., and White, R. H.: Stratosphere-Troposphere Exchanges of Air Mass and Ozone Concentration in the Last Glacial Maximum, Journal of Geophysical Research: Atmospheres, 127, https://doi.org/10.1029/2021JD036327, 2022.

Wilcox, L. J., Hoskins, B. J., and Shine, K. P.: A global blended tropopause based on ERA data. Part II: Trends and tropical broadening, Quarterly Journal of the Royal Meteorological Society, 138, 576–584, https://doi.org/10.1002/qj.910, 2012a.

Wilcox, L. J., Hoskins, B. J., and Shine, K. P.: A global blended tropopause based on ERA data. Part I: Climatology, Quarterly Journal of the Royal Meteorological Society, 138, 561–575, https://doi.org/10.1002/qj.951, 2012b.

World Meteorological Organization (WMO): Definition of the tropopause, WMO Bulletin, 6, 136–138, 1957.

World Meteorological Organization (WMO): Scientific assessment of ozone depletion, 2002, 498pp, World Meteorological Organisation Global Ozone Research and Monitoring Project - Report No.47, Geneva, Switzerland, 2003.

Xian, T. and Homeyer, C. R.: Global tropopause altitudes in radiosondes and reanalyses, Atmospheric Chemistry and Physics, 19, 5661–5678, https://doi.org/10.5194/acp-19-5661-2019, 2019.

Zambri, B., Solomon, S., Thompson, D. W. J., and Fu, Q.: Emergence of Southern Hemisphere stratospheric circulation changes in response to ozone recovery, Nature Geoscience, 14, 638–644, https://doi.org/10.1038/s41561-021-00803-3, 2021.

Zhang, Y., Rossow, W. B., Lacis, A. A., Oinas, V., and Mishchenko, M. I.: Calculation of radiative fluxes from the surface to top of atmosphere based on ISCCP and other global data sets: Refinements of the radiative transfer model and the input data, Journal of Geophysical Research: Atmospheres, 109, 2003JD004 457, https://doi.org/10.1029/2003JD004457, 2004.

Zängl, G. and Hoinka, K. P.: The Tropopause in the Polar Regions, Journal of Climate, 14, 3117–3139, https://doi.org/10.1175/1520-0442(2001)014<3117:TTITPR>2.0.CO;2, 2001.

Škerlak, B., Sprenger, M., and Wernli, H.: A global climatology of stratosphere–troposphere exchange using the ERA-Interim data set from 1979 to 2011, Atmospheric Chemistry and Physics, 14, 913–937, https://doi.org/10.5194/acp-14-913-2014, 2014.